Electrochemical study of zinc-substituted nickel hydroxide

Cécile Tessier, Christiane Faure, Liliane Guerlou-Demourgues, Cathy Denage, Georges Nabias, Claude Delmas

Electrochemical Study of Zinc-Substituted Nickel Hydroxide

Cécile Tessier[1,3], Christiane Faure[1], Liliane Guerlou-Demourgues[1], Catherine Denage[1], Georges Nabias[2] and Claude Delmas[1]

[1] *Institut de Chimie de la Matière Condensée de Bordeaux-CNRS and Ecole Nationale Supérieure de Chimie et Physique de Bordeaux, 33608 Pessac Cedex, France*
[2] *Ecole Nationale Supérieure de Chimie de Montpellier, 34296 Montpellier Cedex 5, France*
[3] *SAFT-Direction de la Recherche, 33074 Bordeaux Cedex, France*

Abstract :
The electrochemical behavior of α- and β(II)-type zinc-substituted nickel hydroxides is studied during a galvanostatic cycling in a KOH electrolyte. It is shown that these materials exhibit very stable capacities during long-term cycling. When using an 8 M KOH electrolyte, the β(III)/β(II) system is stabilized, after the initial formation of γ-type phases during the first charges. The higher the amount of zinc in the starting material, the faster this stabilization occurs. The substitution of zinc for nickel is also shown to delay the formation of the γ-phase upon charge, when various KOH electrolytes, with increasing concentrations, are successively used. A model is proposed to explain these results; it is based on several processes, occurring simultaneously either via the solution or through solid-state reactions, with a partial loss of zinc.

Nickel hydroxide has been extensively studied during the last century because of its use as an active material in alkaline batteries. Various elements are commonly substituted for nickel to improve the electrochemical behavior of the hydroxide. For this purpose, the use of zinc was recently developed, more especially in Ni//MH batteries. This substitution is reported to shift the redox potential to higher values,[1-4] to improve the cycling reversibility,[1,3] to stabilize the capacity upon cycling, but to lower the capacity recovered on discharge at the beginning of the cycling.[1-5] Nevertheless, the capacity in the presence of zinc becomes higher, after numerous cycles, than that obtained without any substituting element. A Sanyo patent[6] also points out the stabilizing effect of zinc, which prevents the capacity loss consecutively to a deep discharge. Moreover, several authors report the ability of zinc to inhibit the formation of the γ-phase upon overcharge.[5,7-12] This last point is of great interest for commercial use, because it prevents the electrode swelling, which is responsible for shortening the life of batteries. Finally, several studies mention that the presence of zinc increases the oxygen evolution potential,[2-4,10] and leads to a better chargeability of the active material.

Nickel hydroxide exists either as β(II)-$Ni(OH)_2$ or as a hydrated phase designated by α-$Ni(OH)_2$. The structure of β(II)-$Ni(OH)_2$ can be described as a packing, along the *c* axis, of NiO_2 slabs made of edge-sharing NiO_6 octahedra. Protons are located in tetrahedral sites in the interslab space, just below or above the oxygen atoms. The structure of α-$Ni(OH)_2$ derives from that of β(II)-$Ni(OH)_2$ by intercalation of one layer of water molecules as well as of anions in the interslab space. β(II)-$Ni(OH)_2$ is oxidized to β(III)-NiOOH by deintercalation of one proton and one electron. Upon overcharge of the battery, the β(III)-phase can be converted into a γ-type phase [$H_xK_yNiO_2 \cdot zH_2O$ ($x,y < 1$)]. Various models have been proposed to explain the battery discharge from the γ phase: (*i*) formation of the α-phase, which is unstable in alkaline solution and is rapidly transformed into a β(II)-phase through a dissolution, nucleation, and growth process,[13,14] and (*ii*) direct transformation into the β(II)-phase via a solid-state process, which was unambiguously shown by electron microscopy.[15] Because the average oxidation degree of nickel ions is 3.5 in γ-type phases, 1.5 electrons are theoretically exchanged during the reduction to α [against only one for the β(III)/β(II) system, as mentioned above].

In our laboratory, a recent study has been devoted to a structural investigation of zinc-substituted nickel hydroxide.[16] It has been shown that the β(II)-type phase is stable up to 15% Zn [atomic ratio $100 \cdot Zn/(Ni + Zn)$] and that zinc ions are substituted for nickel within octahedral sites of the slab. The α-type phase is stable for substitution amounts ranging from 20 to 50% zinc. It presents a turbostratic structure with an interslab distance of 8.4 Å. The zinc cations are located in tetrahedral sites, in the interslab space, each of these tetrahedra shares one face with a vacant octahedron of the slab. The presence of carbonate ions, linked by only one of their oxygen atoms to nickel or zinc cations, has also been highlighted.

In another study dealing with aging tests in 8 M KOH and with chemical cycling of zinc-substituted nickel hydroxide,[17] it has been shown that (*i*) an Ostwald ripening process occurs during the aging test of the β(II)-type phases in concentrated KOH, which leads to the growth of crystallites via a dissolution, nucleation, and growth process, and (*ii*) α-phases are transformed into β(II)-phases via the solution. In both cases, a partial zinc loss occurs during the dissolution. During the chemical cycling, redox reactions have been shown to occur in the solid state, with a partial loss of zinc during a strong oxidation, *i.e.*, when the γ-phase is formed. Successive strong oxidation-reduction cycles, starting from the $\alpha_{25\%Zn}$ phase, allow a β(II)-phase to be obtained via reactions in the solid state, with a partial zinc loss during each strong oxidation. The resulting β(II)-phase must therefore contain octahedral vacancies within the slab.

The present paper deals with the electrochemical behavior of α- and β-(II)-type zinc-substituted nickel hydroxide. The structural evolution of materials with zinc amounts ranging from 0 to 35% Zn was investigated, during a galvanostatic cycling in a KOH electrolyte. Two kinds of studies were carried out; the first one deals with a detailed investigation of the electrochemical cycling in 8 M KOH, whereas the second one concerns the influence of the electrolyte concentration on the electrochemical behavior. The results are discussed on the basis of the preliminary aging and chemical cycling tests.

Experimental

Zinc-substituted nickel hydroxides were obtained by precipitation. 200 mL of a 1 M metal salt solution ($NiSO_4$ and $ZnSO_4$ in the appropriate ratio) were dropped into 300 mL of a 2 M NaOH solution at 25°C. The pH value was thus maintained equal to 14 throughout the precipitation. The precipitate was then washed with deionized water, until the washing water pH reached a steady value of 8-9, before being dried for 15 h at 60°C.

X-ray diffraction (XRD) patterns were obtained with a Siemens D5000 diffractometer (Cu Kα). Most of them were recorded with a scan step of 0.04°(2θ) for 25 s. Some of them, recorded for 7 s/0.04°, were smoothed.

In order to perform scanning electronic microscopy (SEM), a 2 nm layer of platinum was sputtered on the electrodes. Micrographs

* Electrochemical Society Active Member.
z E-mail: delmas@icmcb.u-bordeaux.fr

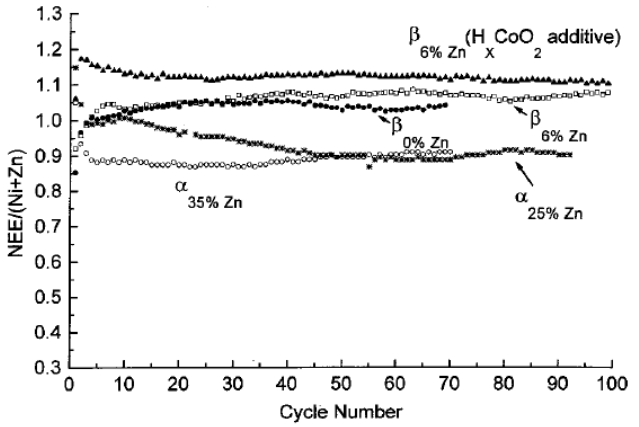

Figure 1. Evolution of the NEE per (Ni + Zn) atom, during a galvanostatic cycling, at the C/5 rate, in 8 M KOH, for the $\beta_{0\%Zn}$, $\beta_{6\%Zn}$, $\alpha_{25\%Zn}$, and $\alpha_{35\%Zn}$ materials (with graphite as the electronic conductor additive). For comparison, the evolution of the NEE/(Ni + Zn), for an electrode constituted of $\beta_{6\%Zn}$ with H_xCoO_2 as additive, is also shown.

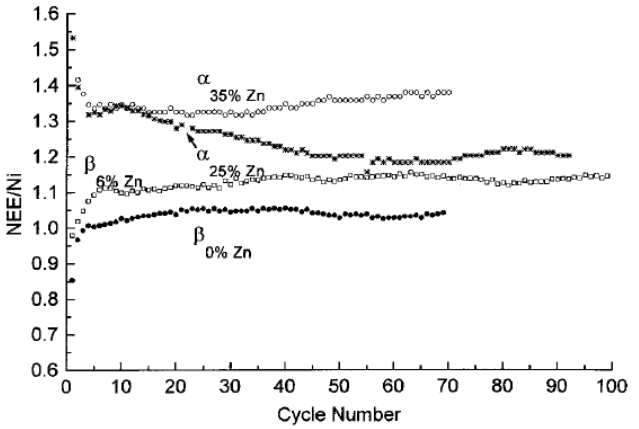

Figure 2. Evolution of the NEE per Ni atom, during a galvanostatic cycling, at the C/5 rate, in 8 M KOH, for the $\beta_{0\%Zn}$, $\beta_{6\%Zn}$, $\alpha_{25\%Zn}$, and $\alpha_{35\%Zn}$ materials.

were recorded with a field emission Hitachi S-4500 microscope.

Electrodes for electrochemical tests were prepared by mixing two-thirds by weight of the active material with one-third by weight of graphite, to ensure a good electronic conductivity. 1 wt % of powdered polytetrafluoroethylene was then added to increase the mechanical strength, and the resulting mixture was pasted onto a nickel foam (1 × 5 cm size). The whole electrode was pressed at 1 t/cm^2, placed into a nonwoven tissue, and then between two polyvinylchloride plates. Two sintered cadmium hydroxide electrodes were placed on either side of the positive electrode, their capacity strongly exceeding that of the positive electrode, so as not to limit the cycling of the battery. A galvanostatic cycling was performed. The first charge was carried out for 20 h at the C/10 rate, meaning that the value of the current intensity is such that 10 h are required to exchange the theoretical capacity of the electrodes (based on one electron exchanged per nickel atom). The subsequent discharge, as well as the following cycles, were performed at the C/5 rate, with 6 h long charges and discharges down to 0.9 V *vs.* $Cd(OH)_2/Cd$. The electrolyte was generally an 8 M KOH solution. In some experiments, 2, 4, 6, and 8 M KOH electrolyte solutions were successively used. Cobalt oxyhydroxide was used as an electronic conductor additive, instead of graphite, in some punctual experiments. This additive is added to the positive electrode mixture, via a solution, in the form of cobalt sulfate, which is transformed into the hydroxide in the alkaline medium, and then irreversibly transformed into the cobalt oxyhydroxide, which exhibits metallic conductivity (H_xCoO_2) during the first charge of the battery.[18] Cobalt oxyhydroxide is commonly used by battery manufacturers as an additive in the nickel hydroxide electrode; it has the ability of forming an electronic conductor film on the grains of active material, thus greatly improving the performances of the battery.[8]

Results and Discussion

In the following, each phase is designated by its structural type, α or β, followed by the atomic ratio used in the synthesis [100 · Zn/(Ni + Zn)].

Evolution of the capacity in 8 M KOH as a function of zinc amount.—The evolutions of the number of electrons exchanged (NEE) per (Ni + Zn) atom and per Ni atom for various zinc compositions, are represented in Fig. 1 and 2, respectively. The NEE/(Ni + Zn) value is interesting from the application point of view, because the presence of electrochemically inactive zinc influences the specific capacity. For comparison, the evolution of the NEE/(Ni + Zn) value of an electrode, with H_xCoO_2 used as the additive instead of graphite, is also shown in Fig. 1. Meanwhile, the evolution of the NEE per nickel ion, shown in Fig. 2, is representative of the influence of zinc amount in the material, on the ability of each nickel ion to reach a high oxidation degree on charge, and to be reduced on subsequent discharge. For each material, several experiments were performed and one battery, representative of the average electrochemical behavior, is presented for discussion.

When the active starting material is a β(II)-type phase, a progressive increase of the NEE can be seen during the first five to ten cycles, corresponding to the activation period. In the presence of the cobalt additive, this period is reduced to two cycles, which is much shorter, as a result of the more homogeneous distribution of the electronic conductor. On the contrary, the cycling of α-type phases is characterized by an initial decrease in capacity. For $\alpha_{25\%Zn}$, this decrease is going on slowly until the 40th cycle. For all materials, the capacity is stabilized during a long-term cycling, after this initial evolution.

The curves in Fig. 1 show that the NEE/(Ni + Zn) for the electrode with $\beta_{6\%Zn}$ (graphite as electronic conductor) is similar to that obtained with $\beta_{0\%Zn}$, at the beginning of the cycling, whereas this value is higher for the zinc-substituted β(II)-phases after 30 cycles. This is in good agreement with the literature.[3] The value of NEE/(Ni + Zn) is still improved for the $\beta_{6\%Zn}$ phase in the presence of the cobalt additive. It reaches a stabilized value of 1.1, which corresponds to 282 mAh/g of (Ni,Zn) hydroxide and to 531 mAh/g of Ni. Nevertheless, it should be noticed that, in industrial batteries, the increase in capacity with the zinc amount does not seem to be so obvious. This different behavior may be due to the fact that spherical nickel hydroxide that is used in industrial batteries is prepared with a peculiar method, different from that used in the present work. Industrial zinc-doped nickel hydroxide is indeed obtained via the decomposition of zinc and nickel ammoniacal complexes, coprecipitated by NaOH in the presence of NH_3, whereas zinc-substituted nickel hydroxides, presently studied, are directly precipitated in NaOH.

As a result of the larger amount of zinc (which is electrochemically inactive), in α-phases than in β(II)-phases, the values of NEE/(Ni + Zn) are lower for α-type phases than for β(II)-type ones. Actually, Fig. 2 shows that the NEE/Ni value increases with the amount of zinc in the active material. The largest stabilized value (1.37) is observed for the $\alpha_{35\%Zn}$ material; it corresponds to 628 mAh/g of Ni. This latter value compares favorably with the capacity of 410 mAh/g of Ni found by Dixit *et al.* for an $\alpha_{40\%Zn}$ material.[19]

Structural evolution of the β(II)-type phases upon cycling in 8 M KOH.—XRD patterns of electrodes with $\beta_{6\%Zn}$ as the active material, at different steps of the cycling, in the charged and discharged state, are shown in Fig. 3, in comparison with that of the starting material. At the beginning of the cycling, during the first three cycles, a γ-phase is formed on charge (C1, C2, and C3). The X-ray diffractogram of the γ-phase exhibits a quite narrow (003) line, indicating that the crystallites are built up of a significant number of slabs. During the respective subsequent discharges (D1, D2, and D3), a mixture of the remaining γ-phase and of a poorly crystallized β(II)-phase is obtained. Actually, the small diffraction line at $2\theta = 66.5°$, which was indexed as (110), allows the direct calculation of the $a_{hex.}$ parameter, which is very different for reduced phases $\{a_{hex.} = 3.08\ Å(\alpha) - 3.12\ Å[\beta(II)]\}$ and oxidized phases $[a_{hex.} = 2.80\ Å$ for both γ and β(III)]. In the present case, the obtained value shows unambiguously that the β(II)-phase is mixed with a γ-phase, and not with an α-one. The C/5 rate does not allow the complete reduction of the material, therefore, a part of the γ-phase remains in the electrode, probably at the core of the grains and therefore far from the current collector, leading to a residual capacity. Furthermore, electrodes were discharged just down to 0.9 V *vs.* $Cd(OH)_2/Cd$, so that only the first plateau was discharged, not the second one.[20] The relatively good crystallinity of the γ-phase at the end of charge C1, C2, and C3 suggests that the reactions, during the first cycles, mainly occur in the solid state, in good agreement with our previous study of $\beta_{6\%Zn}$ oxidation.[17] This behavior presents analogies with the $\gamma \rightarrow \beta(II)$ transformation in the solid state, which was evidenced by Sac-Epée *et al.*[15] On the basis of our experiments, the intermediate formation of the α-phase on discharge cannot be excluded, both steps $\gamma \rightarrow \alpha \rightarrow \beta(II)$ being solid-state processes. Indeed in our laboratory, the presence of the α-phase was very recently demonstrated, after a very high rate of discharge of a γ-phase, in a very low concentrated KOH electrolyte.[21] Such a process in the solid state is quite reasonable at the scale of one cycle, even if one cannot exclude that a small part of the material may pass into solution at the periphery of the grains. This solid-state process was also evidenced in a previous study concerning aging tests of α-type phases.[17] Moreover, the significant broadening of the (001) line, corresponding to the β(II) phase obtained in discharge in the very first cycles, shows that there are a lot of defects in the material, in agreement with the formation in the solid state.

After 15 cycles, a mixture of γ- and β(III)-phases is obtained on charge (C15), while the subsequent discharge (D15) leads to a biphasic material, β(II) + γ. The amount of remaining γ-phase is very small, and the β(II)-phase is better crystallized than that obtained at the third discharge (D3), as evidenced by a narrower (001) line in the D15 diagram *vs.* the D3 one. This tendency is confirmed at the 63rd cycle; the amount of γ-phase after charge is very small, while the β(II)-phase obtained after discharge is still better crystallized than that obtained at the 15th cycle. These results suggest that a β(II)-phase, different from the uncycled $\beta_{6\%Zn}$ phase, tends to grow upon cycling. Actually, whereas the starting phase is completely oxidized to a γ-phase after the third charge, for the β(II)-phase obtained after a large number of cycles, the oxidation to the γ-phase is gradually prevented. The fraction of the β(II)-phase that is not oxidized to γ upon charge is increased during the cycling. This fraction is cycled between β(II) and β(III), via solid-state reactions, and Ostwald ripening is superimposed on the cycling, leading to a significant growth of crystallites.[22] This latter process was actually evidenced during the aging tests of the $\beta_{6\%Zn}$ phase, in a 8 M KOH solution. One should notice that the change in the XRD patterns gives a tendency for the evolution of relative amounts of the two phases, but that quantitative results cannot be directly extracted from the intensity ratio of the first two diffraction lines.

Figure 4 shows the evolution of the XRD patterns of electrodes, manufactured with the $\beta_{0\%Zn}$ phase as the starting active material, recovered in the charged state, at various steps of the cycling, in comparison with the diagram of the starting material. The evolution

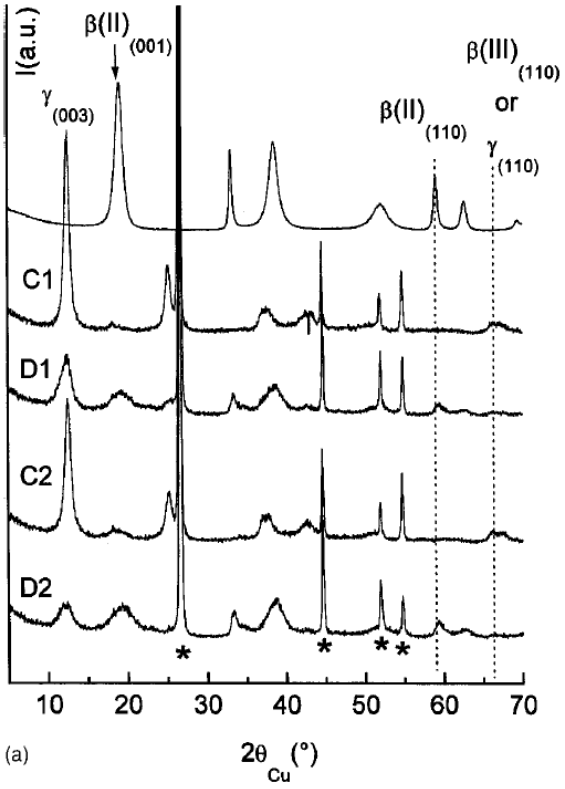

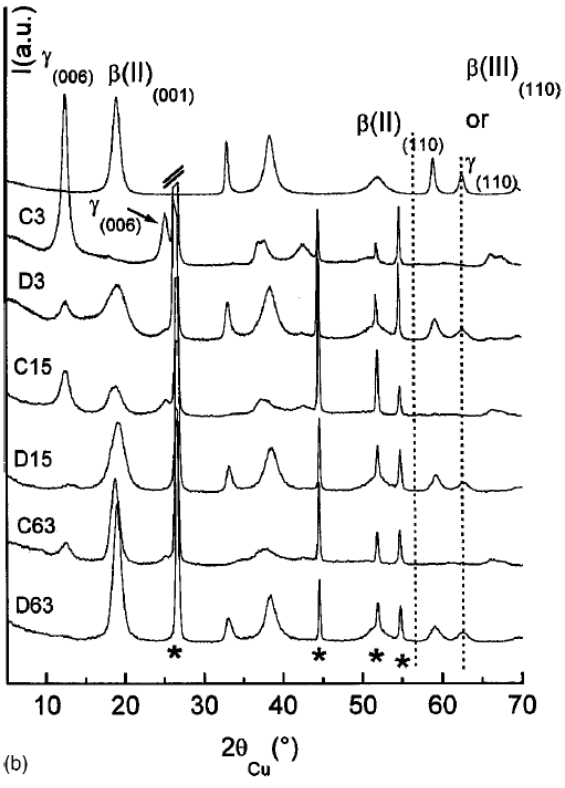

Figure 3. XRD patterns of the electrodes: (a) after the first and second charges (C1 and C2) and discharges (D1 and D2); (b) after the *n*th charges (C_n) and the *n*th discharges (D_n), in comparison with that of the starting $\beta_{6\%Zn}$ phase. Stars show the diffraction lines of Ni and C, added to the electroactive material.

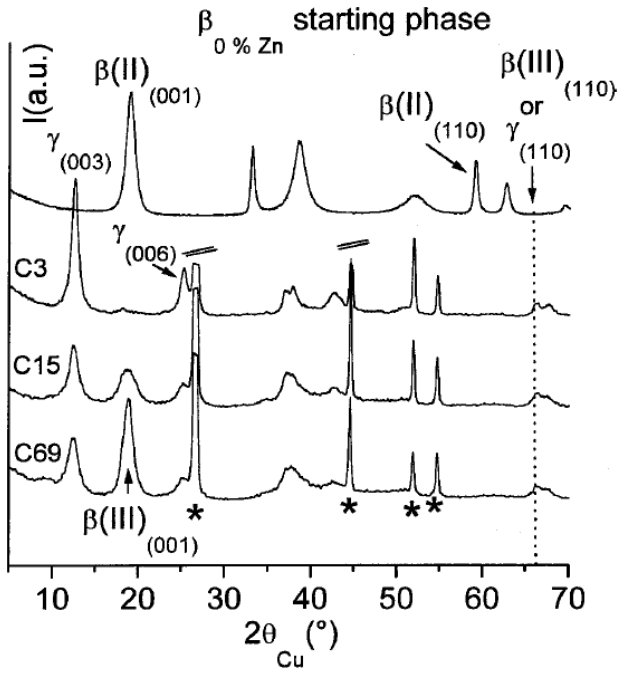

Figure 4. XRD patterns of the electrodes, after the nth charges (C_n), in comparison with that of the starting $\beta_{0\%Zn}$ phase. Stars show the diffraction lines of Ni and C added to the electroactive material.

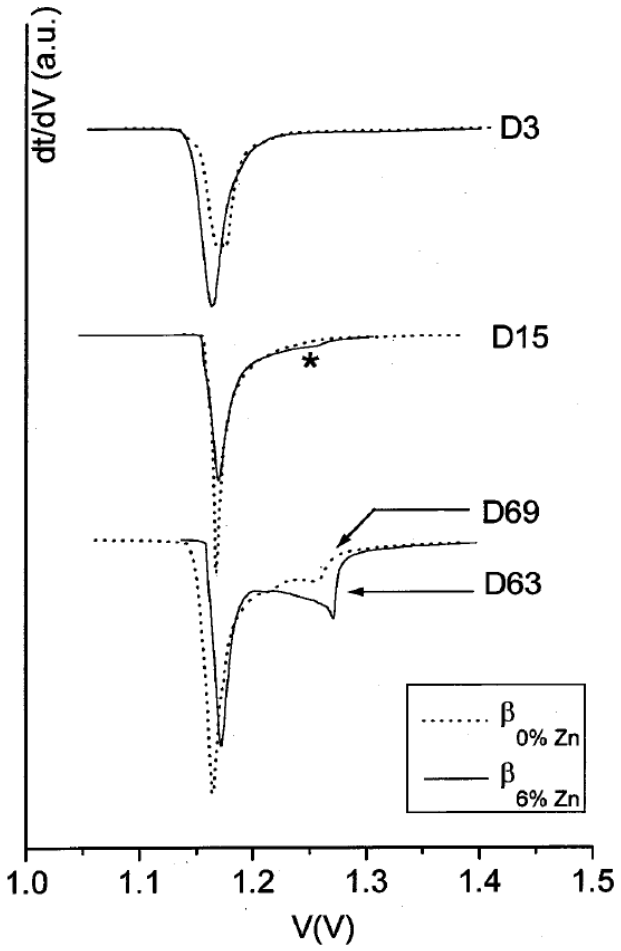

Figure 5. Derivatives of the nth discharge curves (D_n), starting from the $\beta_{0\%Zn}$ phase (dotted line) and from the $\beta_{6\%Zn}$ phase (continuous line).

of the patterns shows, as a general trend, a behavior similar to that obtained with $\beta_{6\%Zn}$. Therefore, only the diagrams relative to the charged state are presented for $\beta_{0\%Zn}$. A well-crystallized γ-phase is obtained after the third charge (C3): after the 15th and 69th charges, a mixture of γ- and β(III)-phases is obtained, the amount of β(III)-phase increasing with the cycle number. A comparison of the γ/β(III) molar ratio, for the phases with 0 and 6% zinc compositions, shows that the β(III) → γ transformation, in charge, is much more limited with the $\beta_{6\%Zn}$ phase, because the amount of the γ-phase after 69 cycles is significant for the cycling with the $\beta_{0\%Zn}$ material.

Derivatives of the discharge curves at the third and 15th cycles, and at the end of the cycling, for electrodes with $\beta_{0\%Zn}$ or $\beta_{6\%Zn}$ as active materials, are compared in Fig. 5. On this kind of curve, the γ/α system is usually characterized by a low-potential peak, around 1.16-1.18 V, and the β(III)/β(II) system by a higher potential peak, around 1.23-1.25 V, these two potential domains being related to the reversible potentials of the two corresponding redox systems, determined by Barnard.[23] At the third discharge, only the γ/α system is present, in good agreement with the XRD results (C3 in Fig. 3 and 4). At the 15th discharge, the low-potential peak is asymmetric toward high-potential values, which shows a non-negligible participation of the β(III)/β(II) system. The asymmetry is more pronounced for the electrode with $\beta_{6\%Zn}$ as the active material, for which a peak starts to form around 1.25 V (see the star in Fig. 5). At the end of the cycling, a large contribution of the β(III)/β(II) system is highlighted. It is clearly more pronounced for the $\beta_{6\%Zn}$ phase than for the $\beta_{0\%Zn}$ one, in good agreement with the XRD results again.

As a conclusion, starting from the β(II)-phases, the electrochemical cycling and the XRD patterns lead to the conclusion that the starting β(II)-phase is completely oxidized to a γ-phase during the very first charge, while a β(II)-phase is formed during the corresponding discharge. Actually, in a first step, the γ-phase must be electrochemically reduced to β(II) (direct formation or via the α-phase). The relatively well-crystallized state of the γ-phase, obtained after the third charge, suggests that the previous reaction occurs in the solid state. The β(II)-phase that is obtained after the reduction gives rise to β(III) or γ, during the subsequent charge, with a progressive transformation of the γ/α system to the β(III)/β(II) one upon cycling. The stabilized cycling within the β(III)/β(II) system allows for the growth of the crystallites. This evolution toward the β(III)/β(II) system is more pronounced with $\beta_{6\%Zn}$ than with $\beta_{0\%Zn}$. The very peculiar shape of the derivative (D63 in Fig. 5) should be noted in the case of the zinc-substituted system. Several contributions appear in the 1.19-1.27 V range, which shows that, even if the XRD pattern shows only one β(II)-type phase, several materials, with different compositions or cationic distributions, are involved in the cycling process. This point is discussed in detail in the general discussion.

Structural evolution of the $\alpha_{25\%Zn}$ phase upon cycling in 8 M KOH.—XRD patterns of electrodes with $\alpha_{25\%Zn}$ as the active material, at different steps of the cycling, in the charged and discharged state, are shown in Fig. 6, in comparison with that of the starting material. After the third charge, a poorly crystallized γ-type phase, with an interstratified structure, is obtained. The interreticular distances corresponding to the first two diffraction lines (dotted lines on curve C3) are not in the 2:1 ratio, suggesting an interstratified structure. Such a material was reported to be obtained during a strong oxidation of the $\alpha_{25\%Zn}$ phase.[17] On the subsequent discharge (D3), a mixture of an α-phase (interslab distance d = 8.2 Å) and of a poorly crystallized β(II)-phase, which is also interstratified, is obtained. The lines at 1.57 and at 1.54 Å (zoom), which correspond to

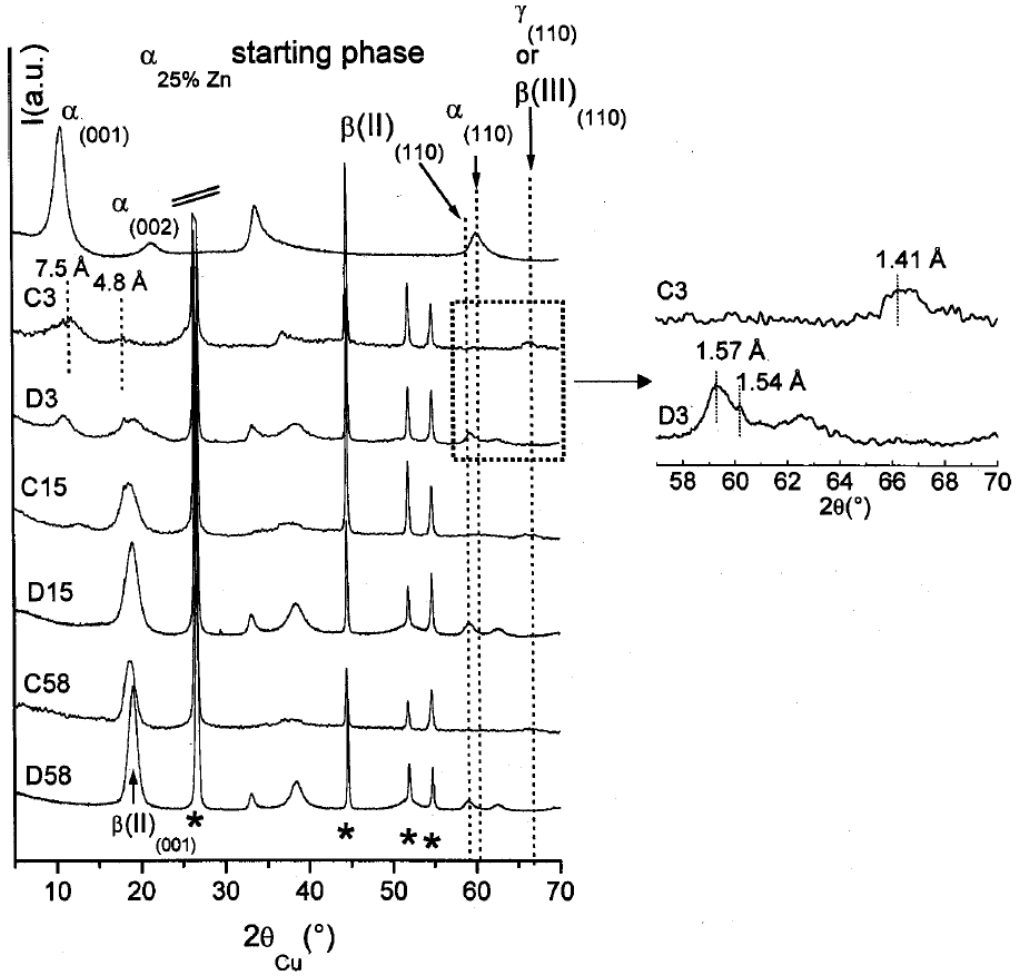

Figure 6. XRD patterns of the electrodes, after the *n*th charges (C_n) and the *n*th discharges (D_n), in comparison with that of the starting $\alpha_{25\%Zn}$ phase. Stars show the diffraction lines of Ni and C added to the electroactive material.

the d_{110} distances in the two materials, are indeed simultaneously present in the XRD patterns. This behavior suggests solid-state reactions. It is in good accord with the results obtained after successive strong oxidation-reduction chemical cycles, starting from $\alpha_{25\%Zn}$, which were shown to lead to a progressive γ/α to β(III)/β(II) transformation, in the solid state, via intermediate interstratified materials.[17] Meanwhile, an aging test of the $\alpha_{25\%Zn}$ phase in 8 M KOH solution, which was carried out for 44 h (*i.e.*, the duration required to perform the three first electrochemical cycles) led to a mixture of α- and β(II)-phases via the solution. In fact, since the α-phase is only present in the reduced state, the kinetics of the dissolution reaction during the cycling cannot be compared with those occurring during the aging tests. Nevertheless, this experiment clearly shows a tendency of dissolution of the material. This suggests that a second process, occurring via the solution, must be involved, in addition to the transformation in the solid state.

Very small traces of γ-phase remain together with the prevailing β(III)-phase after the 15th charge. After 58 cycles, the γ/α system has completely disappeared in favor of the β(III)/β(II) one. As in the case of the β(II)-phases as the starting material, the crystallization state of the β(II)-phase obtained after discharge is improved, cycle after cycle.

Derivatives of the third, 15th, and 58th discharges are represented in Fig. 7. A low potential peak, together with a high potential one, can be seen at the third discharge, which indicates that two redox systems may be involved in the electrochemical process. This is in good agreement with the XRD results, which show after the third charge, an interstratified γ-type phase, constituted of β(III)- and γ-type slabs, which are likely to correspond to the high and low potential peaks, respectively. For the 15th and 58th cycles, a low potential peak is clearly predominant, which could *a priori* be the result of the reduction of the γ-phase into an α-phase. Such an attribution seems unreasonable because the β(III)/β(II) system was shown, by XRD, to be largely prevailing at the 15th cycle, and because no trace of γ was detected after the 58th charge. The origin of this peak is discussed later.

Scanning electronic microscopy (SEM).—Cycled electrodes, with the $\alpha_{25\%Zn}$ phase as active material, were characterized by SEM, in comparison with the starting material and with an uncycled electrode, which was aged for one week in a 8 M KOH solution (Fig. 8). The $\alpha_{25\%Zn}$ phase is constituted of thin platelets (150-500 Å in diameter) with ill-defined outlines. After the third charge (Fig. 8a) and the subsequent discharge (Fig. 8b), the material presents a habitus that is similar to that of the starting material, but with slightly better defined outlines. Some small hexagonal platelets with diameters around 300 Å can also be seen. The similarity in habitus suggests that the main process occurs in the solid state, during these redox reactions. Nevertheless, a partial process via the solution cannot be totally excluded, which may explain the improved definition of the outlines *vs.* the starting material. After 15 cycles (Fig. 8c), hexagonal platelets with well-defined outlines are obtained. Their

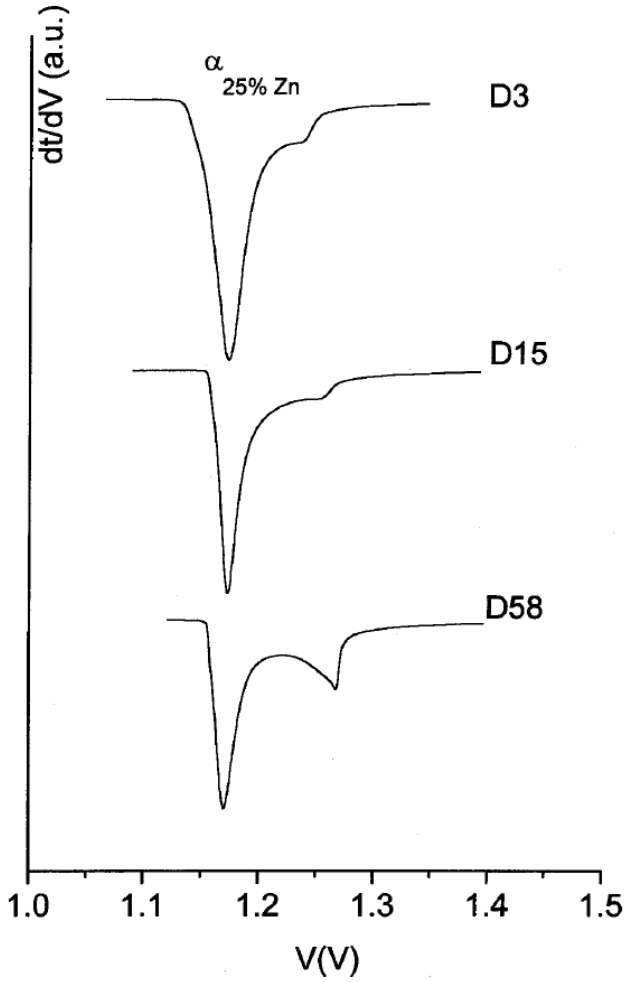

Figure 7. Derivatives of the *n*th discharge curves (D_n), starting from the $\alpha_{25\%Zn}$ phase.

size (300-800 Å diam and 100-200 Å thickness) is significantly higher than the average size of the particles in the starting material, or in the electrode after three cycles. The micrograph in Fig. 8c shows a habitus very similar to that of the uncycled electrode, which was aged for one week in 8 M KOH (Fig. 8d). This shape evolution suggests that a process of dissolution, nucleation, and growth also occurs in the material during the electrochemical cycling. This is consistent with XRD, in Fig. 6, which shows a narrowing of the diffraction lines of the β(II)-phase after the 15th cycle.

To sum up, results obtained by XRD are in good agreement with those deduced from the SEM study. Both methods show that two processes occur simultaneously, one of them occurring in the solid state, whereas the second one implies a dissolution step. At the time scale of one cycle, the solid-state process prevails and is just a small part of the material involved in the Ostwald ripening. Nevertheless, one can assume that, after a large number of cycles, the main part of the material has been involved in the Ostwald ripening. Both processes give rise to a β(II)-phase in the discharged state, which leads to the stabilization of the β(III)/β(II) system during subsequent cycles. This stabilization allows the growth of crystallites of the β(II)-type phases, following an Ostwald ripening. It should be noted that the β(II)-phase, formed in the solid state, must be different from the classical one, since it must contain nickel vacancies due to the loss of zinc.

Structural evolution of the $\beta_{0\%Zn}$ and $\beta_{6\%Zn}$ phases upon cycling as a function of the KOH concentration.—The experiments reported in the previous section were performed in conditions, which were favorable to the formation of the γ-phase on charge; a 20% theoretical overcharge was imposed and a concentrated 8 M KOH solution was used as the electrolyte. In these conditions, the γ-phase is formed, on charge, right at the beginning of the cycling, and the transition from the γ/α to the β(III)/β(II) system, which subsequently occurs, is more pronounced when the active material contains zinc, in substitution for nickel. In the present section, the experiment consists in an initial cycling in a low-concentration of KOH electrolyte (2 M), which allows the activation of the material, but prevents the formation of the γ-phase on charge. Afterward, the electrolyte was removed and replaced by a more concentrated one. In this way, 4, 6, and 8 M concentrated KOH electrolytes were successively used. The aim of the investigation was to study the appearance of the γ-phase, on charge, when using the $\beta_{6\%Zn}$ phase as the active material, in comparison to the $\beta_{0\%Zn}$ one. The evolution with cycling of the NEE per (Ni + Zn) atom, for the $\beta_{6\%Zn}$ phase, is compared to that of the $\beta_{0\%Zn}$ one, in Fig. 9. Figure 10 shows the derivatives of some discharge curves, the fifth and 13th ones, in 2 M KOH, the 14th and 29th, in 4 M KOH, the 31st and 45th, in 6 M KOH, and finally the 50th and 55th ones, in 8 M KOH, were chosen.

For $\beta_{0\%Zn}$, the D5 and D13 derivatives show that only the β(III)/β(II) system (characterized by the exclusive peak in the 1.23-1.26 V range) is involved in the electrochemical reactions in the 2 M electrolyte. For $\beta_{6\%Zn}$, the behavior is the same in the first approximation, but the derivative curves are no more symmetrical, indicating that several closely related materials are clearly present within the electrode. Afterward, each increase in the concentration of KOH immediately leads to an increase in the NEE, due to an increase in the conductivity of the KOH solution. However, any subsequent increase of the NEE value can be related to a structural evolution of the material.

In 4 M KOH, the capacity obtained from the $\beta_{6\%Zn}$ phase is almost stable after the initial small increase in the NEE value. The D14 and D29 derivatives are quite similar (continuous lines in Fig. 10), which confirms the stable behavior, in spite of a very slight increase in the contribution at low potential, for the D29 curve. The very broad shape of the derivative peaks must be noticed; in fact several contributions occur, but their 1.20-1.28 V potential domain allows one to conclude that there is an (almost) exclusive contribution of β(III)/β(II)-type systems. For $\beta_{0\%Zn}$, the value of the NEE continuously increases from the 15th to the 25th cycle, and then stabilizes. This evolution is in good agreement with that of the derivatives. Actually, a low potential peak, corresponding to the γ/α system, clearly appears in the D29 curve, which is not apparent in the D14 one (dotted lines). Indeed, as previously mentioned, the presence of the γ/α system implies a significant increase of the capacity, as compared to the β(III)/β(II) one. The contribution of the γ/α system, in the case of the $\beta_{0\%Zn}$ phase, accounts for the higher NEE value, as compared to $\beta_{6\%Zn}$.

In 6 M KOH, on the contrary, the capacity of the electrode with $\beta_{0\%Zn}$ is almost stable upon cycling, in accordance with the two D31 and D45 derivative curves (dotted lines), which demonstrates a constant contribution of the γ/α system. As shown by the derivative curves, the contribution of the γ/α system is, as expected, still larger in 6 M KOH than in 4 M KOH. Meanwhile, the NEE for the $\beta_{6\%Zn}$ phase progressively increases, while the low-potential peak, characteristic of the γ/α system, appears between the 31st and 45th derivative curves (continuous lines).

In 8 M KOH, both materials exhibit a stable capacity and, accordingly, no modification of the derivative curves throughout the cycling. A contribution of the γ/α system is observed in both cases. This contribution is larger for the $\beta_{0\%Zn}$ phase than for the $\beta_{6\%Zn}$ one, in good agreement with the higher capacity, obtained for the former material, than for the latter one.

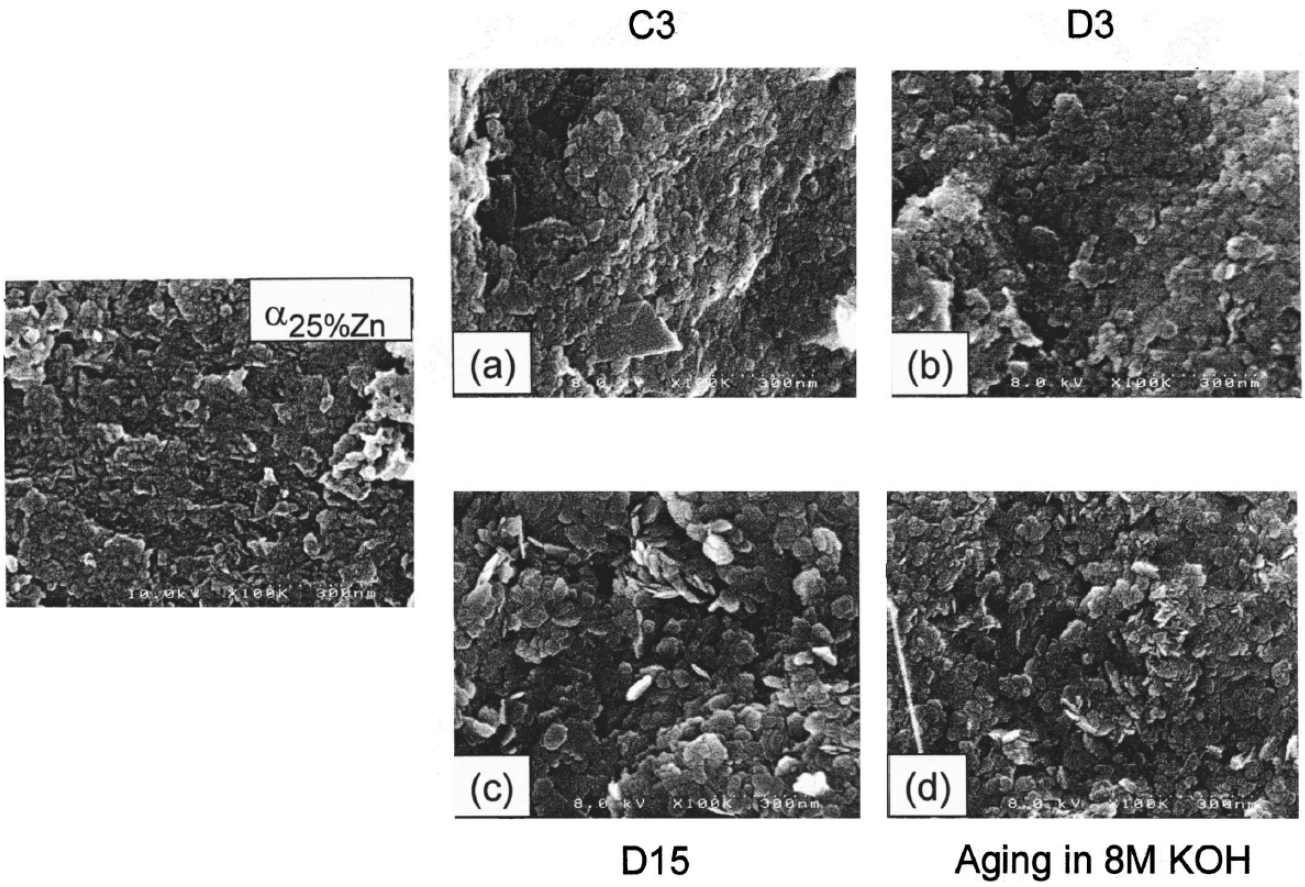

Figure 8. SEM photographs of the electrodes, after the third charge (a) and discharge (b) and after the 15th discharge (c), as compared to that of the starting $\alpha_{25\%Zn}$ material. As a comparison, the SEM photograph of an uncycled electrode, with the $\alpha_{25\%Zn}$ phase as the active material and which was aged for one week in 8 M KOH (d), is also shown.

This experiment shows that zinc, in substitution for nickel in nickel hydroxide, delays the formation of the γ-phase on charge. Actually, with 6% substituting zinc, the γ/α system appears in the KOH electrolyte with a concentration above 6 M, whereas a significant transformation to the γ/α system is already achieved in a 4 M KOH electrolyte, for the $\beta_{0\%Zn}$ phase. It should be noted that the potential of the derivative peak corresponding to the β(III) → β(II) reduction, is higher for $\beta_{6\%Zn}$ than for $\beta_{0\%Zn}$ (Fig. 10), in good agreement with literature.[1]

Discussion

Our experiments show that the presence of zinc, as a substituting element in nickel hydroxide, allows the β(III)/β(II) system to stabilize in good agreement with the literature.[5,7-12] A higher concentration of KOH is necessary to form γ on overcharge, when using $\beta_{6\%Zn}$ instead of $\beta_{0\%Zn}$ as the active material. During cycling in 8 M KOH, after the initial formation of the γ-phase during the first cycles, the long-term cycling, in the presence of zinc, involves a stabilized β(III)/β(II) system. The transformation from the γ/α system to the β(III)/β(II) one is faster for the material with 25% Zn than with 6% Zn. For comparison, for $\beta_{0\%Zn}$, a non-negligible amount of γ remains on charge even after 69 cycles.

Figure 11 tries to summarize schematically the various processes that occur during the electrochemical cycling of the $\beta_{6\%Zn}$ and $\alpha_{25\%Zn}$ phases. The processes involved in the cycling of a β(II)-type phase are different from those starting from an α-type phase, as a consequence of the structural difference between the two kinds of phases. In the β(II)-type phases, zinc cations are located in octahedral sites of the slab, in substitution for nickel, while in the α-phases, they are in tetrahedral sites of the interslab space, associated with nickel vacancies in the slab.

In order to describe the processes presented in Fig. 11, more easily the various experimental results found in this study and in previous ones[16,17] are summarized in Table I.

Evolution of the $\beta(II)_{Zn}$-type phases upon cycling.—During the first charge in 8 M KOH, the β(II)-phase is oxidized to a relatively well-crystallized γ-phase, with the partial loss of zinc. Since the reaction occurs in the solid state, the resulting γ-phase contains octahedral vacancies within the slab, due to the departure of zinc. The subsequent reduction leads to an α-phase, via a reaction in the solid state, in addition to a small fraction of residual γ, with no further loss of zinc. Therefore, octahedral vacancies remain in the α-phase. But this α-phase is unstable in the highly concentrated electrolyte, where it is transformed into the β(II)-phase. Two processes can be envisaged for this transformation, one of them, which is the prevailing one, occurs in the solid-state (process 1 in Fig. 11) and the second one involves a dissolution of the material (process 2 in Fig. 11). The first process leads to a β(II) phase with octahedral vacancies within the slab. During the following charge, this β(II)-phase is oxidized to a relatively well-crystallized γ-phase, which accounts for the presence of such a γ-phase, even at the third cycle, and not only at the first one. Process 2 consists of a transformation via a dissolution and nucleation process. It must lead to very small particles of β(II)-phase, since the growth step has just begun at this

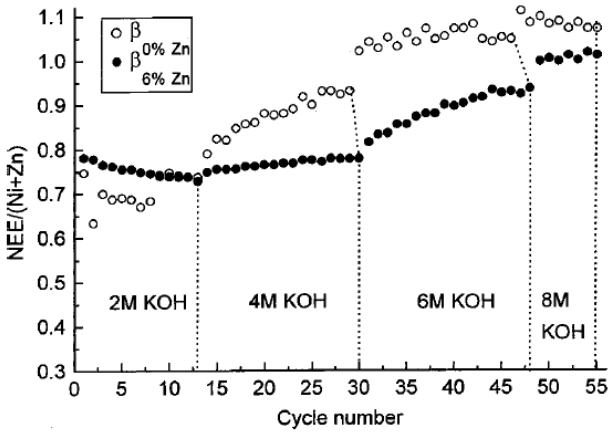

Figure 9. Evolution of the NEE per (Ni + Zn) atom, during an electrochemical cycling of the $\beta_{0\%Zn}$ and $\beta_{6\%Zn}$ phases, in various KOH solutions (2, 4, 6, and 8 M).

stage of the cycling. An extended X-ray absorption fine structure (EXAFS) study, which will be the subject of a forthcoming publication, was performed on a β(II)-phase resulting from the aging of an α-phase.[24] It demonstrates that this β(II)-phase contains zinc cations in tetrahedral sites of the interslab space, which locally prevent the formation of the γ-phase on charge.

Actually, in the case of a nonsubstituted β(II)-phase, the formation of γ, during an overcharge, is due to the oxidation of some nickel ions to Ni^{4+}, related to a strong slab deprotonation. This implies strong electrostatic repulsion between adjacent oxygen planes in the interslab space, which leads to an increase in the interslab distance, and to the intercalation of cations (K^+) in the interslab space.

In the case of β(II) phases, formed upon cycling, zinc cations are located in the interslab space, so that covalent bonds exist between these zinc cations and some oxygen atoms, belonging to the two adjacent oxygen planes of the interslab space. In this case, even if some nickel ions are oxidized to Ni^{4+}, the interslab space cannot be expanded. This explains why the NEE value per nickel atom, obtained during the cycling of the $\beta_{6\%Zn}$ phase, is significantly higher than one, even if the cycling is stabilized in the β(III)/β(II) system. Furthermore, if the ABAB oxygen packing is maintained, each of these zinc cations, located in a tetrahedral site of the interslab space, replaces one proton. This tetrahedron shares three edges with three tetrahedra of the interslab space, which are normally occupied by three protons. In the case of an ideal ABAB oxygen packing, one of these tetrahedra must contain a proton vacancy to ensure electroneutrality; in the two other tetrahedra, protons are strongly destabilized, since they share common edges with the ZnO_4 tetrahedron. Therefore, the chargeability of the material is improved. However, it was shown that zinc-substituted β(II)-type nickel hydroxides contain stacking faults.[16] In the vicinity of these defects, some tetrahedra of the interslab space share one face with one octahedron of the slab.[25] If a zinc ion is located in such a tetrahedron, this involves the occurrence of a nickel vacancy in the octahedron sharing one face with this tetrahedron. The electroneutrality thus implies, either the intercalation of an additional proton, or the oxidation of a neighboring nickel ion to Ni^{3+}, thus improving the electronic conductivity of the β(II)-phase and consequently its chargeability. The subsequent oxidation of this β(II)-phase, leading to the formation of a β(III)-phase, occurs in the solid state with no further loss of zinc, as reported elsewhere, for chemical redox reactions in the β(III)/β(II) system.[17] Therefore, the β(III)-phase also contains zinc in tetrahedral sites of the interslab space. In addition to the previously described two processes, a third one occurs in the discharged state (process 3 in Fig. 11); this is the Ostwald ripening, responsible for the growth of the

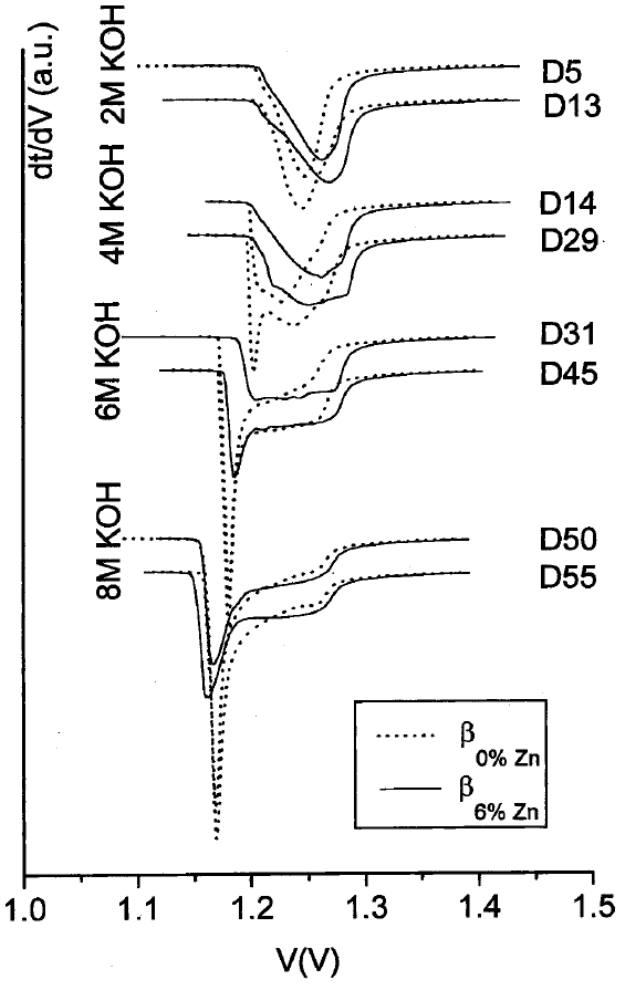

Figure 10. Comparison of the derivatives of discharge curves, at different steps of cycling, for $\beta_{0\%Zn}$ (dotted line) and $\beta_{6\%Zn}$ (continuous line). For each concentration of electrolyte, the derivatives of two discharges are represented, one discharge shortly after the change of electrolyte and one discharge when the capacity obtained in this electrolyte is stabilized.

crystallites of the β(II)-phase. Among these three processes, only the first one retains the material in the γ/α system. However, for the α-phase, formed by the redox reaction of the β(II)-phase with vacancies (resulting from process 1), a fraction of the material follows process 2. As a consequence, cycle after cycle, the whole material will gradually be subject to process 2, and thus it will be stabilized in the β(III)/β(II) system.

Evolution of the α_{Zn}-type phases upon cycling.—Starting from the $\alpha_{25\%Zn}$ phase, an interstratified phase containing γ-type and β(III)-type slabs, designated by I, is obtained after oxidation. The starting material contains zinc cations in tetrahedral sites of the interslab space and octahedral vacancies within the slab; both structural features remain after the oxidation since it occurs in the solid state. The loss of zinc from tetrahedral sites, occurring during this oxidation, leads to a local decrease in the interslab distance, leading to the formation of β(III)-type slabs. The subsequent reduction occurs in the solid state, with no further loss of zinc, and it leads to an interstratified I[α + β(II)] phase [statistical packing of α and β(II) domains]. Two processes can now be considered. The first one (process 4 in Fig. 11) is a dissolution and nucleation process, resulting in the formation of a β(II)-phase, with zinc cations in the interslab space. This β(II)-phase will subsequently behave like that obtained

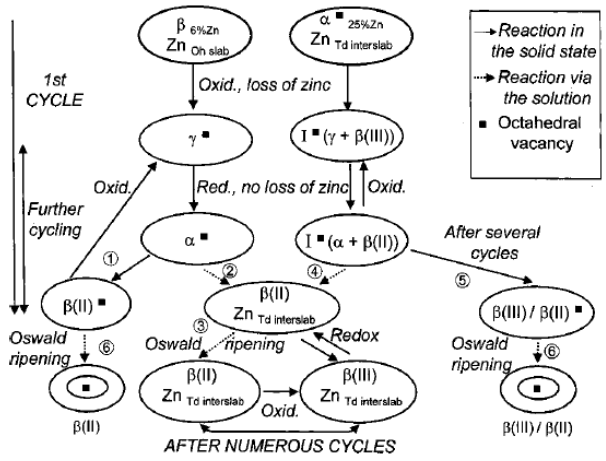

Figure 11. Schematic representation of the processes that occur during the electrochemical cycling of $\beta_{6\%Zn}$ and $\alpha_{25\%Zn}$. Oxid: oxidation; Red.: reduction; I: interstratified material.

while starting from the $\beta_{6\%Zn}$ phase, as already discussed in the previous section. The second process (process 5 in Fig. 11) is a succession of solid-state redox reactions, with a loss of zinc during each oxidation. It leads to a β(II)-phase, due to the departure of intercalated species (zinc ions, carbonate ions, water molecules), with remaining octahedral vacancies within the slabs. For this β(II)-phase, an Ostwald ripening also occurs (process 6 in Fig. 11). Since this process consists in the simultaneous dissolution of the smallest particles and growth of the biggest ones, it leads to a mixture of a classical β(II)-phase and of a β(II)-phase with octahedral vacancies (the heart of the biggest particles, which has not been dissolved). As already suggested, the occurrence of octahedral vacancies, within the slab of the β(II)-phase, should stabilize the β(III)/β(II) system.[17] Actually, after oxidation to β(III), for each Ni^{3+} vacancy within the slab, three nickel ions must be oxidized to Ni^{4+}, without creating strong electrostatic repulsion. Therefore, since there is no deprotonation, this does not imply the increase of the interslab distance. Briefly, the γ-phase is not formed, even if some nickel ions are oxidized to Ni^{4+}, which explains that the value of the NEE per nickel atom is higher than one, even at the end of the cycling, where the β(III)/β(II) system is stabilized.

Comparison of the two systems.—All the processes occurring during the electrochemical cycling of the $\alpha_{25\%Zn}$ phase, directly lead to β(II)-type phases. This explains that the β(III)/β(II) system is stabilized much more rapidly during the cycling of the $\alpha_{25\%Zn}$ phase, than during that of the $\beta_{6\%Zn}$ one. Indeed, for the latter phase, process 1 in Fig. 11 temporally retains a fraction of the material in the γ/α system, which slightly delays the transformation to the β(III)/β(II) system.

The transformation from the γ/α system to the β(III)/β(II) one accounts for the initial decrease in capacity, observed during the electrochemical cycling of α-type phases. Actually, even if the β(II)-phases, formed *in situ* upon cycling either with zinc cations in the interslab space (process 2) or with octahedral vacancies within the slabs (process 5), exchange more than one electron per nickel atom during electrochemical cycling, the capacity does not reach that obtained in the initial γ/α system (1.5 electrons per nickel atom theoretically exchanged). Concerning $\beta_{6\%Zn}$, the initial increase in capacity results from the activation of the material, in addition to the formation of the γ-phase upon charge. Subsequent transformation from the γ/α system to the β(III)/β(II) one does not lead to a decrease in capacity, unlike the case of the $\alpha_{25\%Zn}$.

To sum up, numerous processes occur during the electrochemical cycling of zinc-substituted nickel hydroxide. After the initial formation of the γ-phase, or of an interstratified γ-type phase during the first charges, a combination of these processes leads to a complete transformation from the γ/α system to the β(III)/β(II) one. The various processes imply the formation of different kinds of β(II)-phases, a classical β(II)-phase, a β(II)-phase with zinc in tetrahedral sites of the interslab space, and a β(II)-phase with octahedral vacancies within the slab. The last two kinds of β(II)-phase allow the NEE per nickel atom to reach values higher than one. These three kinds of β(II)-phase probably have three different redox potentials. This explains the very broad discharge derivative curve, observed in Fig. 5 (D63) and in Fig. 10 (D29, continuous line), for the cycling of the $\beta_{6\%Zn}$ phase. More especially, the potential of the β(II)-phase with octahedral vacancies is totally unknown. It could correspond to the low-potential peak, observed in the D58 derivative curve (Fig. 7), at the end of the cycling of the $\alpha_{25\%Zn}$ phase, where only the β(III)/β(II) system is involved. The same low-potential peak is also present in the D63 derivative (Fig. 5); its potential is close to that of the γ/α system but the XRD (Fig. 3) shows that only a very small amount of this system is involved in the cycling. Therefore, one can assume that a part of the low-potential peak corresponds to a β(II)-type phase, with a special cationic distribution.

Conclusions

The electrochemical cycling of zinc-substituted nickel hydroxide in 8 M KOH is very complex. It involves several simultaneous processes, some of them occur in the solid state, whereas some

Table I. Overview of the various phenomena that are involved in the aging in KOH electrolyte and in the chemical and electrochemical cycling, for zinc-substituted β- and α-type nickel hydroxides

	Structure (from Ref. 16)	Aging in KOH (from Ref. 17)	Chemical cycling (Oxidation in NaClO + KOH, reduction in H_2O_2) (from Ref. 17)	Electrochemical cycling (8 M KOH, 20% overcharge) (This work)	Electrochemical cycling as a function of KOH concentration (This work)
β_{Zn}	Zn in octahedral site within the slab	→ β through the solution	Cycling in the β(III)/β(II) system	β → γ upon oxidation during the 1st cycles	Formation of γ delayed in the presence of Zn
		Loss of zinc in the KOH solution	Loss of zinc during the oxidation in the solid-state → Zn vacancy within the slab	Evolution γ/α → β(III)/β(II) in the solid state and also via Ostwald ripening	
α_{Zn}	Zn in tetrahedral site within the interslab space	→ β through the solution	Evolution α → interstratified phases → β(III)/β(II) in the solid state → Zn vacancy within the slab	Evolution α → γ → α → interstratified materials → β(III)/β(II) in the solid state and also via Ostwald ripening.	
	Nickel vacancy within the slab	Loss of zinc in the KOH solution	Loss of zinc		

others imply a dissolution step. These processes lead to the stabilization of the β(III)/β(II) system, during a long-term cycling, this stabilization being faster with $\alpha_{25\%Zn}$ than with $\beta_{6\%Zn}$ as the active material. These effects are related to the involvement of several β(II)-type phases with special structural features (zinc cations in the interslab space and/or octahedral vacancies within the slab).

When the cycling is performed in KOH electrolytes with increasing concentrations, the presence of zinc in the active material also delays the formation of the γ-phase on charge.

The shape of the derivatives of the discharge curves as well as the schematic diagram in Fig. 11 suggest that the same steady state is observed at the end of the cycling, whatever the nature of the starting phase (α or β). The electrode materials contain β(II)-type hydroxides with different cationic distributions, leading to a large extent of electrode potential.

Acknowledgments

The authors thank M. Ménétrier, J. M. Dauchier, and P. Bernard for fruitful discussion, and M. Basterreix and B. Delatouche for their technical support. We gratefully acknowledge the help of the staff of the laboratory in Montpellier for SEM experiments. We are also grateful to SAFT, ANRT, and Région Aquitaine for financial support.

Institut de Chimie de la Matière Condensée de Bordeaux assisted in meeting the publication costs of this article.

References

1. R. J. Doran, in *Proceedings of the International Symposium on Batteries*, Royal Aircraft Establishment, Farnborough, U.K. (1958).
2. D. A. Corrigan and R. M. Bendert, *J. Electrochem. Soc.*, **136**, 723 (1989).
3. M. E. Unates, M. E. Folquer, J. R. Vilche, and A. J. Arvia, *J. Electrochem. Soc.*, **135**, 25 (1988).
4. M. E. Unates, M. E. Folquer, J. R. Vilche, and A. J. Arvia, in *Proceedings of the Symposium on Nickel Hydroxide Electrodes*, D. A. Corrigan and A. H. Zimmerman, Editors, PV 90-4, p. 134, The Electrochemical Society Proceedings Series, Pennington, NJ (1990).
5. A. Yuan, S. Cheng, J. Zhang, and C. Cao, *J. Power Sources,* 77, 178 (1999).
6. A. Yamawaki, S. Nakaori, T. Hamamatsu, and Y. Baba, Sanyo Electric Co. Ltd., Eur. Pat. 96301881.7 (1996).
7. B. B. Ezhov and O. G. Malandin, *J. Electrochem. Soc.,* **138**, 885 (1991).
8. M. Oshitani, K. Takashima, and Y. Matsumara, in *Proceedings of the Symposium on Nickel Hydroxide Electrodes*, D. A. Corrigan and A. H. Zimmerman, Editors, PV 90-4, p. 197, The Electrochemical Society Proceedings Series, Pennington, NJ (1990).
9. M. Oshitani, T. Takayama, K. Takashima, and S. Tsuji, *J. Appl. Electrochem.,* , **16**, 403 (1986).
10. M. Oshitani, M. Watada, T. Tanaka, and T. Iida, in *Hydrogen and Metal Hydride Batteries*, P. D. Bennett and T. Sakai, Editors, PV 94-27, p. 303, The Electrochemical Society Proceedings Series, Pennington, NJ (1994).
11. M. Oshitani, H. Yufu, and K. Hasegawa, Yuasa Battery Co, Ltd., Eur. Pat. 89303952.9 (1989).
12. D. H. Fritts, in *The Nickel Electrode*, R. G. Gunther and S. Gross, Editors, PV 82-4, p. 175, The Electrochemical Society Proceedings Series, Pennington, NJ (1982).
13. H. Bode, K. Dehmelt, and J. Witte, *Electrochim. Acta,* **11**, 1079 (1966).
14. S. Le Bihan and M. Figlarz, *J. Cryst. Growth,* **13-14**, 458 (1972).
15. N. Sac-Epée, M. R. Palacin, A. Delahaye-Vidal, Y. Chabre, and J. M. Tarascon, *J. Electrochem. Soc.,* **145**, 1434 (1998).
16. C. Tessier, L. Guerlou-Demourgues, C. Faure, A. Demourgues, and C. Delmas, *J. Mater. Chem.,* **10**, 1185 (2000).
17. C. Tessier, L. Guerlou-Demourgues, C. Faure, M. Basterreix, G. Nabias, and C. Delmas, *Solid State Ionics,* **133**, 11 (2000).
18. Sorapec, Fr. Pat. 2670709 (1992).
19. M. Dixit, P. Vishnu Kamath, and J. Gopalakrishnan, *J. Electrochem. Soc.,* **146**, 79 (1999).
20. C. Léger, C. Tessier, M. Ménétrier, C. Denage, and C. Delmas, *J. Electrochem. Soc.,* **146**, 924 (1999).
21. P. H. Haumesser, C. Denage, L. Guerlou-Demourgues, and C. Delmas, To be published.
22. W. Oswald, *Z. Phys. Chem.*, **34**, 495 (1900).
23. R. Barnard, C. F. Randell, and F. L. Tye, *J. Appl. Electrochem.,* **10**, 109 (1980).
24. L. Guerlou-Demourgues, C. Tessier, P. Bernard, and C. Delmas, To be published.
25. C. Tessier, P. H. Haumesser, P. Bernard, and C. Delmas, *J. Electrochem. Soc.,* **146**, 2059 (1999).